Biosensors and Bioelectronics 41 (2013) 615–620

Contents lists available at SciVerse ScienceDirect

Biosensors and Bioelectronics

journal homepage: www.elsevier.com/locate/bios

Amplified electrochemiluminescence detection of DNA-binding protein based on the synergy effect of electron and energy transfer between CdS nanocrystals and gold nanoparticles

Jing Wang, Wei-Wei Zhao, Hong Zhou, Jing-Juan Xu *, Hong-Yuan Chen

State Key Lab of Analytical Chemistry for Life Science, School of Chemistry and Chemical Engineering, Nanjing University, Nanjing 210093, China

ARTICLE INFO

Article history:
Received 27 July 2012
Received in revised form
19 September 2012
Accepted 21 September 2012
Available online 28 September 2012

Keywords:
Electrochemiluminescence
Electron transfer
Energy transfer
Synergy effect
DNA-binding protein

ABSTRACT

In this work, we firstly enunciated the presence of synergy effect between the electron and energy transfer in an electrochemiluminescence (ECL) system involving the CdS NCs and Au NPs, based on which an amplified ECL biosensor was constructed for sensitive detection of DNA–protein interactions. Specifically, Au NPs modified on electrode, following by assembled probe DNA. Then the modified GCE was hybridized with SiO_2@CdS/DNA conjugates. With DNA duplex as a rigid spacer, Au NPs could not only accelerate the electron transfer but also produce the surface plasma resonance upon excited ECL of CdS NCs. However, the enhanced ECL could be greatly suppressed by the binding of target protein. The prepared biosensor possesses excellent analytical performance with the linear range of target protein from 0.015 to 150 nM.

1. Introduction

DNA–protein interactions play important roles in cellular processes, such as transcription, replication, recombination, and repair (Boon et al., 2002; Ren et al., 2000). The TATA-binding protein (TBP) is a general transcription factor that binds specifically to a DNA sequence called the TATA box and bends the DNA duplex with 30–102° (Delgadillo et al., 2009; Kim et al., 1993; Williams et al., 2006). There have been some efforts in recent years in monitoring such proteins including fluorimetric (Parkhurst et al., 2002), colorimetric (Ou et al., 2010), surface enhanced resonance Raman scattering (Bonham et al., 2007) and electrochemical methods (Boon et al., 2002; Chang and Li, 2009; Gorodetsky et al., 2008). When every strategy has distinct advantages, each one suffers from its own limitations such as poor sensitivity or high equipment cost. Hence, the development of alternative assays for sensitive detecting DNA binding proteins and probing DNA–protein interactions would be desirable.

Electrochemiluminescence (ECL) technique has been developed as one of the most versatile methods for the detection of various biological recognition events due to its inherent low background, satisfactory sensitivity, good temporal and spatial control, and hence better analytical performances (Miao, 2008; Richter, 2004). Of numerous ECL emitter materials, semiconductor nanocrystals (S-NCs) has in the past decade drawn a wide attention among the community because of their unique advantages including high quantum yields of fluorescence, size or surface trap-control luminescence as well as good stability (Lei and Ju, 2011; Zhao et al., 2012a,2012b; Zhou et al., 2011a). For bioanalysis, ECL of S-NCs have been extensively used for different analytes, such as immune molecules, DNA oligonucleotides, enzyme inhibitors, cells and some small molecules (Shan et al., 2010,2011; Tian et al., 2012; Wang et al., 2012a; Zhou et al., 2011b). To date, however, ECL based monitoring of DNA–protein interaction has been rare reported. On the other hand, for bioanalysis application, Au nanoparticles (Au NPs) seem to be the most versatile and extensively studied material among the various NPs due to their large surface area, good biocompatibility and excellent electron transfer (Cui et al., 2004). In ECL, numerous works have reported the utilization of Au NPs to amplified the ECL intensity of S-NCs (Han et al., 2010; Jie et al., 2010,2011). However, in all these reports, the enhanced ECL signal was exclusively explained by its effect for increasing the electrode surface and boosting the electron transfer between the electrode and the ECL reactants.

Luminescence resonance energy transfer (LRET) is a powerful technique for probing changes in the distance between donors and acceptors, and is ideal for the sensitive detection of molecular binding events in response to interactions with a particular target molecule (Perroy et al., 2004; Zhao et al., 2010). As the energy

* Corresponding author.
E-mail address: xujj@nju.edu.cn (J.-J. Xu).

0956-5663/$ - see front matter © 2012 Elsevier B.V. All rights reserved.
http://dx.doi.org/10.1016/j.bios.2012.09.041

transfer between the excitons in the S-NCs and plasmons in the metal surface occurs, the optical properties of S-NCs near the metal surface could be modified significantly by controlling the nanoscale-localized energy transfer (Matsuda et al., 2008; Maye et al., 2010). Previous studies have shown that interactions with proximal metal NPs (Au, Ag NPs) can greatly affect the photoluminescence (PL) intensities of S-NCs, in which PL intensity of the S-NCs is either enhanced or diminished due to the competition between field enhancement and nonradiative energy transfer (Anger et al., 2006; Jin and Gao, 2009). Lately, interesting results have also been reported about its serving as a new biosensor strategy in ECL (Shan et al., 2009; Wang et al., 2011; Zhou et al., 2011a, 2011b). In detail, when CdS NCs and Au NPs were in close proximity upon certain ECL conditions, the interparticle energy transfer would occur. It means the energy transfer process exists in such ECL system that involves the S-NCs and Au NPs. Given the research of energy transfer in ECL is still in its infancy, the further study of energy transfer for advanced ECL bioanalysis, e.g. probing DNA–protein interaction, is surely interesting.

Very recently, we developed an ECL biosensor based on the K-doped graphene as an enhanced electron transfer substrate for amplified detection of TBP (Wang et al., 2012b). This work is based on the change of direct electron transfer process prior and after the biorecognition events. Since the energy transfer has demonstration as a feasible sensing principle, of particular interest here is the possibility of integrating electron and energy transfer into ECL platform to exploit the innovative sensing format for advanced ECL bioassay of DNA–protein interaction. If possible, it will significantly advance the incorporation of new bioanalysis strategy into ECL biosensors as well as provide great opportunities for examination of the DNA–protein interaction from a different technical perspective.

With the special research attention, this work presents our latest findings of the synergy effect of electron and energy transfer between S-NCs and noble metal NPs, based on which the sensitive ECL detection of DNA–protein interaction was successfully realized. As shown in Scheme 1, the SiO_2 nanopartical as a traditional carrier was employed to load large number of CdS NCs with the aim to amplify the ECL signal. This SiO_2@CdS nanocomposite then reacted with amino modified ssDNA 1. Au NPs coated onto the GCE, following by anchored probe DNA (ssDNA 2) via the Au–S bond. Then the modified GCE was hybridized with SiO_2@CdS/DNA conjugates to form the DNA duplex that contains the TATA box between ssDNA 1 and ssDNA 2. With the dsDNA as a rigid spacer, Au NPs were bridged to SiO_2@CdS nanocomposite for enhancement of electron transfer and stimulation of Au NPs SPR by ECL emission. In the presence of target protein TBP, the synergy effect of Förster resonance energy transfer (FRET) quenching and impeded electron transfer and steric hindrance would greatly suppress the ECL signal. This strategy provides a viable mechanism for ECL biosensor protocol and opens a different horizon for analysis of DNA–protein interactions.

2. Experimental section

2.1. Materials

Labeled DNA oligonucleotides were purchased from Shenggong Bioengineering Ltd. Company (Shanghai, China). The sequences of these oligonucleotides employed are given as follows:

Amino modified DNA 1:

ss-DNA 1: 5′-NH_2-$(CH_2)_6$-AGGAGGGCGCGCAGGTCTTTTATA-CGGCGG-3′

Thiol modified complementary DNA 2:

ss-DNA 1: 5′-SH-$(CH_2)_6$-CCGCCG***TATAAAAG***ACCTCGCCGCCCT-CCT-3′

Amino modified bio bar code DNA 3:

bbc-DNA: 5′-NH_2-$(CH_2)_6$-ACGCTAGCTATGCTT-3′

(ss-DNA 1 were complementary with ss-DNA 2. Bold italic portion indicated the TATA binding protein binding site).

SiO_2 NPs (99.5%, 20 ± 5 nm) were obtained from Aladdin reagent Inc (Shanghai, China). TATA binding protein (Constituents: 20% Glycerol, 20 mM Tris HCl, 100 mM Potassium chloride, 1 mM DTT, 0.2 mM EDTA, pH 8.0) was ordered from Abcam website. 3-aminopropyl-triethoxysilane (APTS), 1-methylimidazol, 3-mercaptopropionic acid (MPA), N-(3-dimethylaminopropyl)-N′-ethyl-carbodiimide hydrochloride (EDC) and N-hydroxysuccinimide (NHS), 3-mercapto-1-hexanol (MCH), bovine serum albumin (BSA) were purchased from Sigma-Aldrich (St. Louis, MO) and used without further purification. All other reagents were of analytical grade and used as received. Millipore ultrapure water (resistivity ≥ 18.2 MΩ cm) was used throughout the experiment.

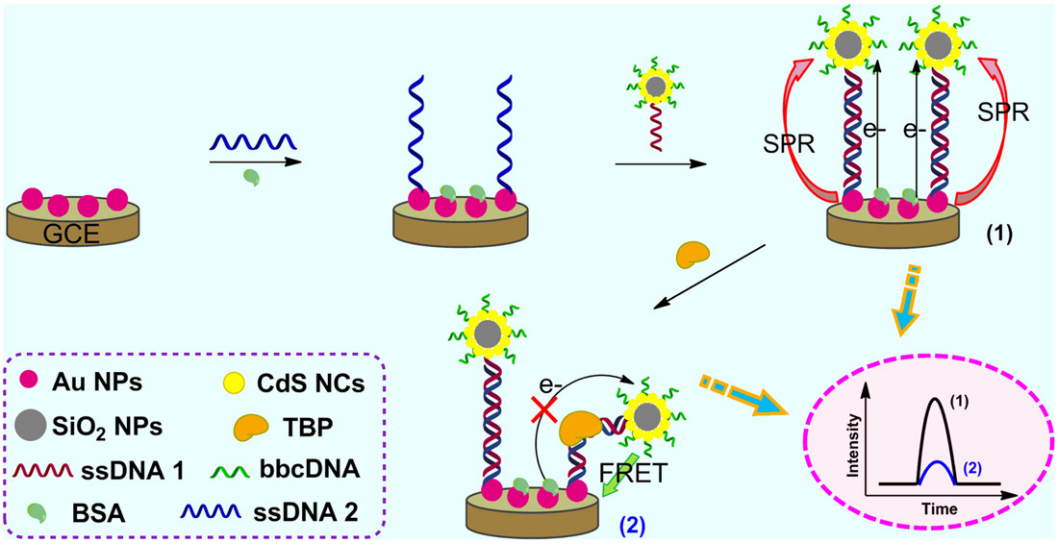

Scheme 1. The analytical procedure of the amplified ECL TBP assay.

2.2. Apparatus

The electrochemical measurements were recorded with CHI 660A electrochemical workstation (Shanghai CHI Instruments Co., China). The ECL emission measurements were conducted on a model MPI-A electrochemiluminescence analyzer (Xi'An Remax Electronic Science &Technology Co. Ltd., Xi'An, China) at room temperature, and the voltage of the PMT was set at −500 V in the process of detection. All experiments were carried out with a conventional three-electrode system. The working electrode was a 3 mm diameter glassy carbon electrode (GCE), Pt wire and SCE electrode served as the counter and reference electrodes, respectively.

Transmission electron microscopy (TEM) was performed with a JEOL model 2000 instrument operating at 200 kV accelerating voltage. The UV–vis absorption spectra were obtained on a Shimadzu UV-3600 UV–vis–NIR photospectrometer (Shimadzu Co.).

2.3. Preparation of SiO_2@CdS/DNA conjugates

The average size of 5 nm CdS NCs were synthesized as our previous works (Wang et al., 2011). For the preparation of CdS NCs coated SiO_2 nanoparticles, 0.02 g of SiO_2 nanoparticles were first dispersed in 2 mL of ethanol and treated with 0.4 mL of APTS. After stirring for 6 h, the suspension was centrifuged and washed with ethanol repeatedly for four times, and the amino-functionalized SiO_2 nanoparticles were obtained. Then, the amino-functionalized SiO_2 were dispersed in 1 mL of the terminal carboxylic acid group activated CdS NCs, which derived from the reaction in 1.0 mL of 0.1 M 1-methylimidazol aqueous solution (pH 7.4) containing 20 mg EDC and 10 mg NHS for 2 h at 4 °C. The mixed suspension was stirred at 4 °C for 12 h. Unbound CdS NCs were removed by successive centrifugation and washing with water several times. Finally, the as-prepared SiO_2@CdS nanocomposites, which had the same color as CdS NCs itself, were obtained and dispersed in water.

To generate SiO_2@CdS/DNA conjugates, the ssDNA 1 and bbc-DNA modified with amino at their 5′-end were used, and the molar ratio between the oligonucleotides and SiO_2@CdS was optimized. In detail, different volumes of 1 μM bbc-DNA were added to 100 μL of SiO_2@CdS NPs, after shaking gently for 12 h, they covalently attached through the binding reaction of activated carboxylic acid group and amino group. Then centrifuged at 10,000 rpm for 30 min, the supernatant was taken for UV–vis absorbance detection. It was found that the absorbance markedly increased when the volume of the bbc-DNA was more than 1 mL, indicating that the reaction of DNA with SiO_2@CdS NPs was saturated after 1 mL. Thus, 900 μL of 1 μM bbc-DNA and 100 μL of 1 μM ssDNA 1 were the optimized values. The bbc-DNA was used as dilute DNA to lower the density of ssDNA 1, which not only improved the sensitivity but also blocked the active sites of SiO_2@CdS nanocomposite. Finally, the SiO_2@CdS/DNA conjugates were kept in 0.1 M PBS containing 0.5 M NaCl (pH 7.4) at 4 °C before use.

2.4. Preparation of ECL biosensor for assay of TBP

Au NPs with average diameter 5 ± 1 nm were prepared through the reduction of $HAuCl_4$ by sodium borohydride ($NaBH_4$) according to the reported methods with slight modifications (Gole and Murphy, 2004; Shan et al., 2009).

The fabrication procedure of the ECL biosensor is illustrated in Scheme 1. The GCE was pretreated before modification by polishing its surface with successively finer grades sand papers and then polished to mirror smoothness with aqueous slurries of alumina powders on a polishing silk. The GCE was thoroughly rinsed with water and then sonicated in ethanol and ultrapure water in turn. The fresh GCE was treated with cysteine, and then soaked in 200 μL Au NPs solution for 2 h. The modified GCE was immersed in 0.1 M PBS containing 1 μM ssDNA 2 for 12 h, following by reacted with 2 wt% BSA to block the nonspecific binding sites of the Au NPs for 2 h. Finally, SiO_2@CdS/DNA conjugates were anchored on the modified GCE via the base complementation of ssDNA 1 and ssDNA 2 for 40 min at 37 °C. The electrode surface was rinsed with 0.1 M PBS buffer after each step to remove nonspecifically adsorbed species.

For the detection of target protein TBP, the biosensor was incubated with variable concentration of TBP, which could result in different ECL signaling for quantization. Before and after the incubation, the ECL responses of the biosensor were both recorded in 0.1 M PBS (pH 8.0) containing 0.05 M $K_2S_2O_8$ as a coreactant. The linear scan potential was applied with a scan rate of 100 mV s^{-1}, and the voltage of the PMT was set at −500 V.

3. Result and discussion

3.1. Characterization of SiO_2@CdS/DNA conjugates

Fig. 1 shows the UV–vis spectroscopy of the formed SiO_2@CdS/DNA conjugates. As shown in curve a, pure SiO_2 particles aqueous suspension did not exhibit any evident absorption peak in the wavelength scope. However, the absorption peak of ca. 470 nm corresponding to CdS NCs appeared in curve b, from which the particle size was calculated to be about 6.1 nm (Yu et al., 2003). In light of the characterized absorption of purine and thymine bases, the appearance of 260 nm peak in curve c indicated the functionalization of DNA onto the SiO_2@CdS nanocomposites. Moreover, the inset of Fig. 1 displays the typical TEM images of pure SiO_2 particles (above) and the SiO_2@CdS nanocomposites (below). Apparently, the pure SiO_2 particles showed homogeneous size distribution and smooth surfaces with the exterior diameter about 20 nm, while the SiO_2@CdS nanocomposites exhibited rough surfaces with exterior diameter of 27 ± 2.5 nm. This difference indicated that plenty CdS NCs were successfully decorated on the surface of SiO_2 particles. Such conjugates have previously demonstrated about 7-fold enhancement of the ECL signal than the pure CdS/DNA conjugates (Wang et al., 2012b).

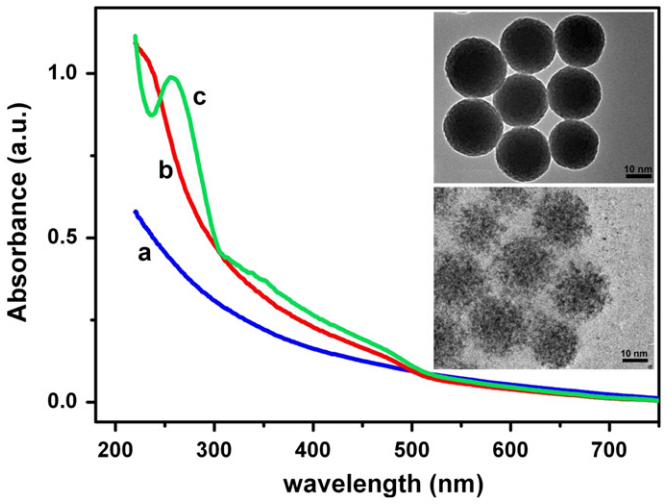

Fig. 1. UV–vis absorption spectra of: (a) SiO_2 particles, (b) SiO_2@CdS nanocomposites, and (c) SiO_2@CdS/DNA conjugates. The inset is the TEM images of pure SiO_2 particles (above); and the SiO_2@CdS nanocomposites (below).

3.2. Characterization of ECL biosensor

Fig. 2A shows the progressive ECL intensity responses of the modified electrodes. Au NPs modified GCE did not show any ECL emission (curve a), offering a good background for the following analysis. Curve b suggested that the further anchoring of probe ssDNA 2 and BSA could not generate the ECL signal. After assembling SiO_2@CdS/DNA conjugates, upon the potential scan with an initial negative direction, the loaded CdS NCs in conjugates were reduced to $CdS^{-\bullet}$ by the charge injection transferred along the DNA duplex. Meanwhile, the coreactant $S_2O_8^{2-}$ was electrochemically reduced to the strong oxidant $SO_4^{-\bullet}$. Thereafter, $SO_4^{-\bullet}$ reacted with the $CdS^{-\bullet}$ to produce an excited state of CdS NCs (CdS*) and emitted light (Jie et al., 2007; Myung et al., 2002). Noteworthily, a dramatic rise of ECL response (ca. 17200) appeared at curve c, which may be due to the interparticle interaction between the Au NPs and CdS NCs. Specifically, Au NPs not only acted as conductor to accelerate the electron transfer but also as producer to generate SPR upon the light illumination. To better clarify, a control experiment without Au NPs was then carried out (curve d). It was demonstrated that the ECL intensity of the SiO_2@CdS/DNA conjugates was only a quarter of that involved the use of Au NPs, indicating the great rise of ECL should be attributed to the presence of Au NPs. Incidently, it has been well proved that Au NPs can increase the effective surface area of the electrode and enhance the rate of electron transfer (Divsar and Ju, 2011; Zhang et al., 2008). Similar effect was also displayed in this work, as indicated by the cyclic voltammograms (CV) shown in Fig. 2A inset curve a and b.

For the efficient excitation of the SPR, the spectra overlap between the ECL emission spectra of the CdS NCs and absorption spectra of Au NPs is essential (Zhao et al. 2012c). In Fig. 2B curve a depicts the typical ECL emission spectrum of the CdS NCs with the emission peak centered at ca. 520 nm, and curve b displayed the absorption spectra of the Au NPs with the maximum plasmon absorption peak at ca. 525 nm. Apparently, the ECL emission of the CdS NCs had a large spectral overlap with the SPR absorption of the Au NPs, which would be beneficial to the inducement of the SPR of the Au NPs and thus affect the subsequent interparticle interaction. In control experiment, MCH, rather than BSA, was selected to adjust the SPR absorption of Au NPs because its negative charge could change the charge density of Au NPs surface. As expected, a larger red shift was observed for the maximum absorption of Au NPs, with the peak at ca. 600 nm (curve c). Such shift would result in the two spectrum overlapped to a lower extent. Fig. 2A, curve e showed that the corresponding ECL exhibited a lower enhancement, which could be attributed to the lower efficiency of energy transfer. Fig. 2A inset (curve a' and b') showed the cyclic voltammograms (CV) corresponding to Fig. 2A (c and e). The similar CV responses demonstrated the identical charge transfer rate of the two Au NPs on the electrode surface and hence the fact that the different increment degree of ECL on the Au NPs and MCH treated Au NPs should be attributed to the different interparticle energy interaction rather than the charge transfer rate. Taken together, these experimental results demonstrated that the overall amplified ECL response was due to the synergy effect of electron and energy transfer between CdS NCs and Au NPs. Unfortunately, in previous similar ECL configuration involving NCs and Au NPs, the influenced ECL was exclusively attributed to the affected electron transfer rate, leaving such mechanism has not been clearly enunciated before.

Given the importance of probing DNA-protein interactions as mentioned before, such synergy effect-based mechanism was then exploited for the ECL determination of target protein. After the specific binding of TBP (100 nM) to the DNA sequence, a sharp decrease ~81.9% of ECL intensity as compared to the initial value was observed as shown by curve b in Fig. 3. Similarly, the control experiment was also performed by incubation the same concentration TBP with the SiO_2@CdS/DNA conjugates directly assembled on the ssDNA modified bare GCE, the ECL intensity only reduced by ca. 46.7% (Fig. 3 inset, curve b'). There were at least three possible reasons for such conspicuous attenuation of ECL signal: (1) The energy transfer influenced ECL of S-NCs related exquisitely with the interparticle distance (Shan et al., 2009). Here, TBP binding with the promoter TATA sequence (TATAAAAG) would induce a $\geq 90^{\circ}$ bending in the DNA duplex (Delgadillo et al., 2009; Parkhurst et al., 1996), leading to the distance between CdS NCs and Au NPs decreased from 10 nm to ~3 nm (3 bases was considered as 1 nm). Our previous work has demonstrated that Förster resonance energy transfer (FRET) quenching was a short-range effect, with the decreasing separation distance, FRET effect was predominated, while the SPR-field enhancement could be negligible (Wang et al., 2011). That is to say some excitation energy of CdS NCs consuming in closely proximal Au NPs through the nonradiative energy transfer

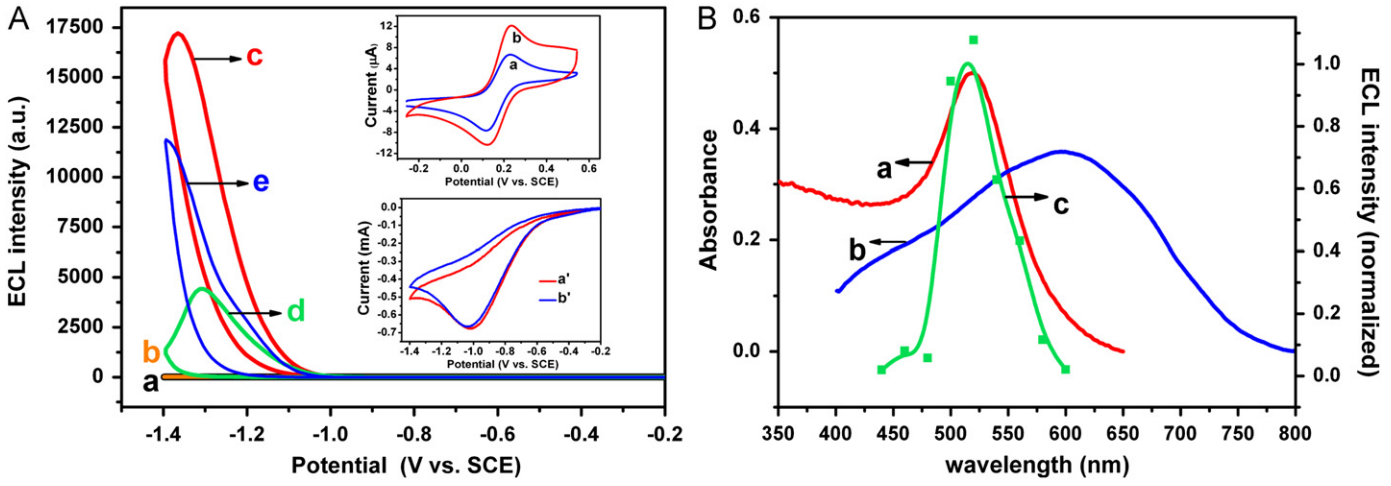

Fig. 2. A: ECL response of (a) the Au NPs modified GCE, (b) assembled with ssDNA 2 and further blocking with BSA, (c) after SiO_2@CdS/DNA composites anchoring, (d) SiO_2@CdS/DNA composites anchored on bare GCE without Au NPs, and (e) SiO_2@CdS/DNA composites anchored on MCH treated Au NPs modified GCE. ECL detection buffer: 0.1 M PBS (pH 7.4) containing 0.05 M $S_2O_8^{2-}$. The inset is the CV responses of: (a) bare, and (b) Au NPs modified GCE in 0.1 M KCl solution containing 5 mM $K_3[Fe(CN)_6]$/ $K_4[Fe(CN)_6]$. Scan rate: 50 mV s^{-1}; (a') SiO_2@CdS/DNA composites assembled on Au NPs modified GCE, (b') composites assembled on MCH treated Au NPs modified GCE in ECL detection buffer. Scan rate: 100 mV s^{-1}. B: (a) UV–vis absorption spectra of Au NPs; (b) ECL spectrum of the CdS NCs obtained by filter plates; and (c) UV–vis absorption spectra of Au NPs treated with MCH.

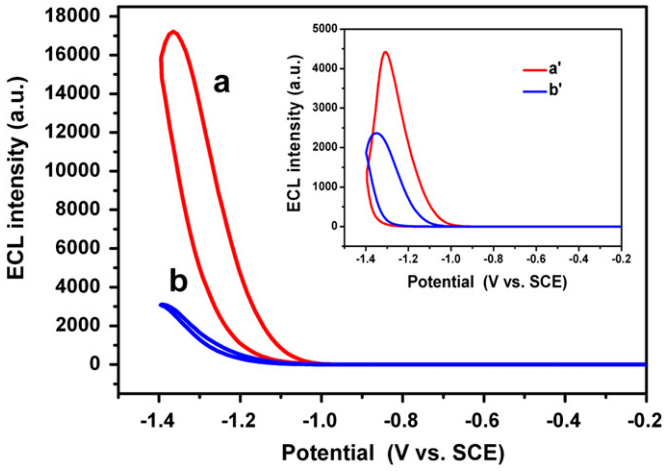

Fig. 3. ECL response of SiO_2@CdS/DNA composites hybridized with ssDNA 2 on Au NPs modified GCE (a) before and (b) after TBP (100 nM) incubation. The inset is the control experiment without Au NPs (a') before and (b') after TBP incubation at the same conditions.

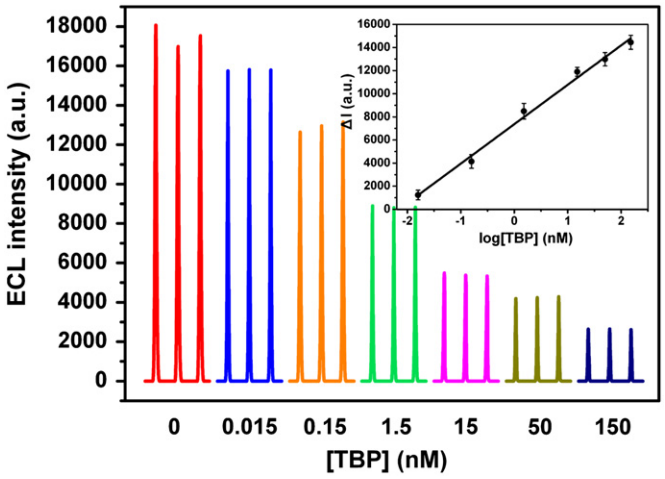

Fig. 4. The ECL signals of the biosensor incubated with different concentrations of TBP (from left to right, 0, 0.015, 0.15, 1.5, 15, 50 and 150 nM, respectively). Inset: the corresponding logarithmic calibration curve. $\Delta I = I_0 - I$, I_0 stands for the ECL signal of the modified electrode before TBP immobilization and I was the final ECL of the electrode after incubation with TBP of elevated concentrations.

could lead the ECL intensity decrease. (2) From the traditional perspective of steric hindrance, the formation of bent DNA–TBP intermediate complexes, as compared with SiO_2@CdS/DNA composites alone, would greatly increase the steric hindrance and hence retard the diffusion of ECL reagents towards the electrode surface. The lowed concentration of electrochemically reduced products would subesequently inhibit the efficiency of ECL emission. (3) TBP binding to its target site could kink the DNA duplex and perturb the base pair stack and further damp the DNA-mediated electron transfer and hence hampered the electrochemical response (Gorodetsky et al., 2008). In our system, the TBP binding could impair the electron transfer along the DNA duplex, which impacted the ECL signal of CdS NCs.

3.3. Analytical performance of ECL biosensor to TBP

Since the degree of ECL signal was directly related to the concentration of TBP, a sensitive ECL biosensor could fabricated by tracking the ECL intensity to monitor the extent of DNA–protein interaction. As shown in Fig. 4, with the increase of the concentration of TBP binding with the DNA duplex, the ECL signal decreased. Fig. 4 inset showed that the ECL decline was proportional to the concentration of target protein in logarithmic scale with the linear range from 0.015 to 150 nm with a correlation coefficient of 0.991 ($n=4$). Due to the synergy effect as stated above, the detection limit of TBP was found at levels down to 5 pM, which was superior to that obtained from the only using of improving electron transfer rate amplification strategy (Wang et al. 2012b).

To reveal the selectivity and specificity of this strategy, contrast experiments were preformed. We measured three other proteins: thrombin (Thro), alpha-fetoprotein (AFP), and lysozyme (Lyso) under the same experimental conditions and at the same concentrations (1.5 nM, 15 nM, and 60 nM). Fig. 5 shows that these proteins could not binding to the TATA box and did not exhibit any great decrease of signal in each group under the same concentration. This comparison essentially suggested that this biosensor was highly selective and had quite an affinity toward the target protein.

The reproducibility of the proposed biosensor for TBP was evaluated. The variation coefficients (ECL response) was 5.92%, which was assessed by assaying 100 nM TBP at four different electrodes independently. Thus, the results demonstrated that the biosensor possessed acceptable reproducibility. Furthermore, we found that this ECL biosensor retained 93.2% of original ECL

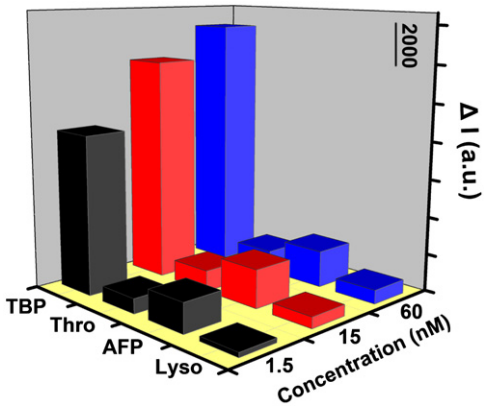

Fig. 5. Selectivity of the proposed biosensor to TBP by comparing it to the interfering proteins: Thro, AFP, Lyso at 1.5, 15, and 60 nM respectively. All ECL responses were recorded in 0.1 M PBS (pH 7.4) containing 0.05 M $S_2O_8^{2-}$ with −500 V PMT. Error bars represent S. D., $n=3$.

response after 15 days of storage in PBS buffer (pH 7.4) at 4 °C, indicating a good stability of the biosensor.

4. Conclusions

In summary, this work firstly demonstrated the existence of synergy effect between the electron and energy transfer process in such ECL systems involving the CdS NCs and Au NPs, based on which an amplified ECL biosensor was constructed for sensitive detection of the DNA binding protein. The work not only supplemented the tradition ECL mechanism to exploit the innovative sensing format for advanced ECL bioassay, but also provided great opportunities for examination of the DNA–protein interaction from a different technical perspective. More generally, integrated electron and energy transfer into ECL platform could serve as a sensing basis for other biorecognition events or biocatalytic transformations.

Acknowledgments

This work was supported by the 973 Program (2012CB932600), the National Natural Science Foundation (No. 21025522 and

21135003) and the National Natural Science Funds for Creative Research Groups (21121091) of China.

References

Anger, P., Bharadwaj, P., Novotny, L., 2006. Physical Review Letters 96 (11), 113002–113004.

Bonham, A.J., Braun, G., Pavel, I., Moskovits, M., Reich, N.O., 2007. Journal of the American Chemical Society 129 (47), 14572–14573.

Boon, E.M., Salas, J.E., Barton, J.K., 2002. Nature Biotechnology 20 (3), 282–286.

Chang, H., Li, J., 2009. Electrochemistry Communications 11 (11), 2101–2104.

Cui, H., Xu, Y., Zhang, Z.F., 2004. Analytical Chemistry 76 (14), 4002–4010.

Delgadillo, R.F., Whittington, J.E., Parkhurst, L.K., Parkhurst, L.J., 2009. Biochemistry 48 (8), 1801–1809.

Divsar, F., Ju, H.X., 2011. Chemical Communications 47 (35), 9879–9881.

Gole, A., Murphy, C.J., 2004. Chemistry of Materials 16 (19), 3633–3640.

Gorodetsky, A.A., Ebrahim, A., Barton, J.K., 2008. Journal of the American Chemical Society 130 (10), 2924–2925.

Han, E., Ding, L., Lian, H., Ju, H., 2010. Chemical Communications 46 (30), 5446–5448.

Jie, G., Liu, P., Wang, L., Zhang, S., 2010. Electrochemistry Communications 12 (1), 22–26.

Jie, G., Wang, L., Yuan, J., Zhang, S., 2011. Analytical Chemistry 83 (10), 3873–3880.

Jie, G.F., Liu, B., Pan, H.C., Zhu, J.J., Chen, H.Y., 2007. Analytical Chemistry 79 (15), 5574–5581.

Jin, Y.D., Gao, X.H., 2009. Nature Nanotechnology 4 (9), 571–576.

Kim, J.L., Nikolov, D.B., Burley, S.K., 1993. Nature 365 (6446), 520–527.

Lei, J., Ju, H., 2011. Trac-Trends In Analytical Chemistry 30 (8), 1351–1359.

Matsuda, K., Ito, Y., Kanemitsu, Y., 2008. Applied Physics Letters 92 (21), 211911.

Maye, M.M., Gang, O., Cotlet, M., 2010. Chemical Communications 46 (33), 6111–6113.

Miao, W., 2008. Chemical Reviews 108 (7), 2506–2553.

Myung, N., Ding, Z.F., Bard, A.J., 2002. Nano Letters 2 (11), 1315–1319.

Ou, L.-J., Jin, P.-Y., Chu, X., Jiang, J.-H., Yu, R.-Q., 2010. Analytical Chemistry 82 (14), 6015–6024.

Parkhurst, K.M., Brenowitz, M., Parkhurst, L.J., 1996. Biochemistry 35 (23), 7459–7465.

Parkhurst, L.J., Parkhurst, K.M., Powell, R., Wu, J., Williams, S., 2002. Biopolymers 61 (3), 180–200.

Perroy, J., Pontier, S., Charest, P.G., Aubry, M., Bouvier, M., 2004. Nature Methods 1 (3), 203–208.

Ren, B., Robert, F., Wyrick, J.J., Aparicio, O., Jennings, E.G., Simon, I., Zeitlinger, J., Schreiber, J., Hannett, N., Kanin, E., Volkert, T.L., Wilson, C.J., Bell, S.P., Young, R.A., 2000. Science 290 (5500), 2306–2309.

Richter, M.M., 2004. Chemical Reviews 104 (6), 3003–3036.

Shan, Y., Xu, J.-J., Chen, H.-Y., 2009. Chemical Communications 46 (8), 905–907.

Shan, Y., Xu, J.-J., Chen, H.-Y., 2010. Chemical Communications 46 (28), 5079–5081.

Shan, Y., Xu, J.-J., Chen, H.-Y., 2011. Nanoscale 3 (7), 2916–2923.

Tian, C.-Y., Zhao, W.-W., Wang, J., Xu, J.-J., Chen, H.-Y., 2012. Analyst 137 (13), 3070–3075.

Wang, J., Shan, Y., Zhao, W.-W., Xu, J.-J., Chen, H.-Y., 2011. Analytical Chemistry 83 (11), 4004–4011.

Wang, J., Zhao, W.-W., Tian, C.-Y., Xu, J.-J., Chen, H.-Y., 2012a. Talanta 89, 422–426.

Wang, J., Zhao, W.-W., Li, X.-R., Xu, J.-J., Chen, H.-Y., 2012b. Chemical Communications 48 (51), 6429–6431.

Williams, S.L., Parkhurst, L.K., Parkhurst, L.J., 2006. Nucleic Acids Research 34 (3), 1028–1035.

Yu, W.W., Qu, L.H., Guo, W.Z., Peng, X.G., 2003. Chemistry of Materials 15 (14), 2854–2860.

Zhang, L.H., Wang, F., Dong, S.J., 2008. Electrochimica Acta 53 (22), 6423–6427.

Zhao, S., Huang, Y., Shi, M., Liu, R., Liu, Y.-M., 2010. Analytical Chemistry 82 (5), 2036–2041.

Zhao, W.-W., Dong, X.-Y., Wang, J., Kong, F.-Y., Xu, J.-J., Chen, H.-Y., 2012a. Chemical Communications 48 (43), 5253–5255.

Zhao, W.-W., Ma, Z.-Y., Yu, P.-P., Dong, X.-Y., Xu, J.-J., Chen, H.-Y., 2012b. Analytical Chemistry 84 (2), 917–923.

Zhao, W.-W., Yu, P.-P., Shan, Y., Wang, J., Xu, J.-J., Chen, H.-Y., 2012c. Analytical Chemistry 84 (14), 5892–5897.

Zhou, H., Liu, J., Xu, J.-J., Chen, H.-Y., 2011a. Analytical Chemistry 83 (21), 8320–8328.

Zhou, H., Liu, J., Xu, J.-J., Chen, H.-Y., 2011b. Chemical Communications 47 (29), 8358–8360.